

Quantifying Spin-Orbit Torques in Antiferromagnet/Heavy Metal Heterostructures

Egecan Cogulu,¹ Hantao Zhang,² Nahuel N. Statuto,¹ Yang Cheng,³ Fengyuan Yang,³ Ran Cheng,^{2,4} and Andrew D. Kent¹

¹*Center for Quantum Phenomena, Department of Physics, New York University, NY 10003, USA*

²*Department of Electrical and Computer Engineering,
University of California, Riverside, CA 92521, USA*

³*Department of Physics, The Ohio State University, Columbus, OH 43210, USA*

⁴*Department of Physics and Astronomy, University of California, Riverside, CA 92521, USA*

(Dated: March 23, 2022)

The effect of spin currents on the magnetic order of insulating antiferromagnets (AFMs) is of fundamental interest and can enable new applications. Toward this goal, characterizing the spin-orbit torques (SOT) associated with AFM/heavy metal (HM) interfaces is important. Here we report the full angular dependence of the harmonic Hall voltages in a predominantly easy-plane AFM, epitaxial c-axis oriented α -Fe₂O₃ films, with an interface to Pt. By modeling the harmonic Hall signals together with the α -Fe₂O₃ magnetic parameters, we determine the amplitudes of field-like and damping-like SOT. Out-of-plane field scans are shown to be essential to determining the damping-like component of the torques. In contrast to ferromagnetic/heavy metal heterostructures, our results demonstrate that the field-like torques are significantly larger than the damping-like torques, which we correlate with the presence of a large imaginary component of the interface spin-mixing conductance. Our work demonstrates a direct way of characterizing SOT in AFM/HM heterostructures.

Recently antiferromagnetic materials have been gathering increasing attention from the spintronics community due to their advantageous properties such as fast spin dynamics, low susceptibility, and magnetic moment compensation [1–4]. Detecting and manipulating antiferromagnetic order electrically is an important milestone for realizing devices based on AFMs [5–9]. It is known that spin-orbit torques (SOT) are one of the most effective ways to manipulate magnetic order in both ferromagnets (FM) and ferrimagnets [10–18]. However, their effectiveness is less well explored and quantified for AFMs. Therefore, characterizing the SOT is crucial for understanding and predicting AFM dynamics. A powerful technique to characterize SOT is harmonic Hall measurements [19, 20]. Although this technique has been used extensively in FM/heavy metal (HM) bilayers, harmonic Hall study of SOT in AFMs remains elusive.

In this work, we use harmonic Hall measurements to characterize the SOT in α -Fe₂O₃/Pt bilayers. SOT are a result of the spin-Hall effect (SHE) in Pt [21, 22], in which a charge current leads to a spin accumulation at the α -Fe₂O₃ interface. SOT can modify the orientation of the AFM Néel vector and this change can be detected electrically because of spin Hall magnetoresistance (SMR) [23, 24]. SMR arises from combination of SHE, interface scattering, and the inverse SHE [25]. Most importantly for our study, SMR manifests as an anisotropy in the resistivity of the Pt and a Hall signal analogous to the planar Hall in ferromagnets [26]. We first characterize the SMR by 1st harmonic response and then SOT from the 2nd harmonic response.

Then, we develop a model of the response that accounts for the magnetic properties of α -Fe₂O₃ and compare the model with the experimental results. By fitting

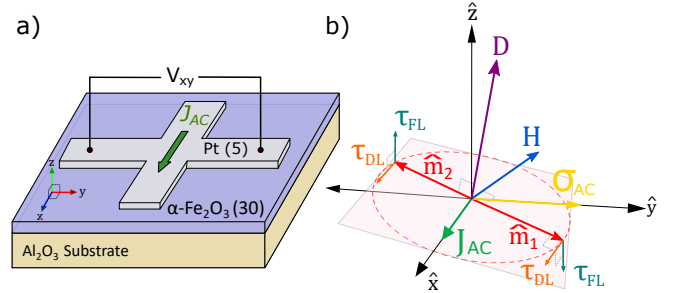


FIG. 1. a) Transverse measurement configuration showing the Pt Hall cross with 5 μ m channel width. An AC current J_{AC} is applied in the \hat{x} -direction, and the transverse voltage V_{xy} is measured with a lock-in amplifier. b) Modeling geometry. \mathbf{D} represents both the DMI vector and the hard axis direction that defines the easy plane. \mathbf{m}_1 and \mathbf{m}_2 are the sublattice moments and \mathbf{H} is the external magnetic field. The spin accumulation σ_{AC} is in the \hat{y} -direction. The resulting spin-orbit torques on the sublattice moments are decomposed into field-like (τ_{FL}) and damping-like components (τ_{DL}).

the data from six measurements together (the 1st and 2nd harmonic response with the field rotated in three orthogonal planes), we extract the amplitudes of the damping-like and field-like torques. Surprisingly and contrary to the case of ferromagnets/heavy metal heterostructures, we find field-like torques to be significantly larger than damping-like torques.

Figure 1(a) shows a schematic of the experimental setup. We perform Hall measurements at 300 K on 30 nm thick epitaxial c-axis oriented α -Fe₂O₃ on Al₂O₃ (0001) substrates capped in-situ with 5 nm thick Pt [8, 20]. The Pt layer is patterned into a $5 \times 15 \mu\text{m}^2$ Hall-cross structure and the Hall voltage is detected with a lock-in am-

plifier with a 953 Hz AC current of 4×10^9 A/m² and 6×10^{10} A/m² used for 1st and 2nd harmonic measurements, respectively.

Figure 1(b) shows the geometry used in our model. The antiferromagnet's hard axis and DMI vector are represented by the same vector \mathbf{D} . The AFM sublattice moment directions are indicated by unit vectors \mathbf{m}_1 and \mathbf{m}_2 . The Néel vector $\mathbf{n} = (\mathbf{m}_1 - \mathbf{m}_2)/2$ lies in the easy plane, which is perpendicular to \mathbf{D} , indicated by the red plane. \mathbf{H} is the applied magnetic field and σ_{AC} is the spin accumulation at the interface caused by \mathbf{J}_{AC} via the SHE. The resulting SOT on the sublattice moments are decomposed into field-like (τ_{FL}) and damping-like components (τ_{DL}). Notice we do not constrain \mathbf{D} to be parallel to the \hat{z} -axis, as canting of the easy plane in AFMs, due to the strain effects from the substrate has been reported [9, 27]. As shown at the top of Fig. 2, \mathbf{H} is rotated in one of the three planes: XY, XZ or YZ, where the current \mathbf{J}_{AC} is in the \hat{x} direction.

Figure 2 shows the full angular dependence of Hall signals (blue points), for all three field scans, at $\mu_0 H = 3$ T together with the model fit (red lines). In the in-plane XY scan, both 1st and 2nd harmonic Hall signals follow smooth trigonometric functions. This is expected because spin-Hall magnetoresistance (SMR) and field-like torques are the main contributors in 1st and 2nd XY scan harmonic signals, respectively. On the other hand, for out-of-plane field rotation experiments—XZ and YZ field scans—the angular dependencies do not follow a simple trigonometric function. A comprehensive model is needed in order to explain all six scans, as we discuss below.

In the sample geometry indicated in Fig. 1(b), an AC current density $\mathbf{J}_{AC}(t) = J_0 \cos \omega t$ generates an oscillating spin accumulation $\sigma_{AC}(t)$ in the \hat{y} direction, which produces SOT on α -Fe₂O₃. The measured Hall voltage V_{xy} arises from the SMR: $V_{xy}(t) = A_x J_0 R_{xy}[\mathbf{n}(\mathbf{J}_{AC}, \mathbf{H})] \cos \omega t$, where A_x is area through which the current flows and has the form $R_{xy} \sim n_x n_y$ [25, 29–32]. Since the current-induced torques only result in a slight deviation of \mathbf{n} from its equilibrium orientation, we can expand the SMR as:

$$R_{xy}[\mathbf{n}(\mathbf{J}_{AC}, \mathbf{H})] = R_{xy}[\mathbf{n}(0, \mathbf{H})] + J_0 \left(\frac{\partial R_{xy}}{\partial \mathbf{n}} \right) \frac{\partial \mathbf{n}}{\partial J_{AC}} \Big|_{(0, \mathbf{H})} \cos \omega t + h.o., \quad (1)$$

where the first term $R_{xy}[\mathbf{n}(0, \mathbf{H})]$ is the SMR, which leads to the first harmonic signal $V_{xy}^{1\omega}(t) = A_x J_0 R_{xy}[\mathbf{n}(0, \mathbf{H})] \cos \omega t$. The second term, which is itself proportional to J_0 , gives rise to the second harmonic response $V_{xy}^{2\omega}(t)$. Therefore, to find the harmonic responses, we need to calculate $\mathbf{n}(0, \mathbf{H})$. $\partial \mathbf{n} / \partial J_{AC}$ is determined by the dynamics of the Néel vector and hence by the dynamics of sublattice magnetic moments, \mathbf{m}_1 and \mathbf{m}_2 .

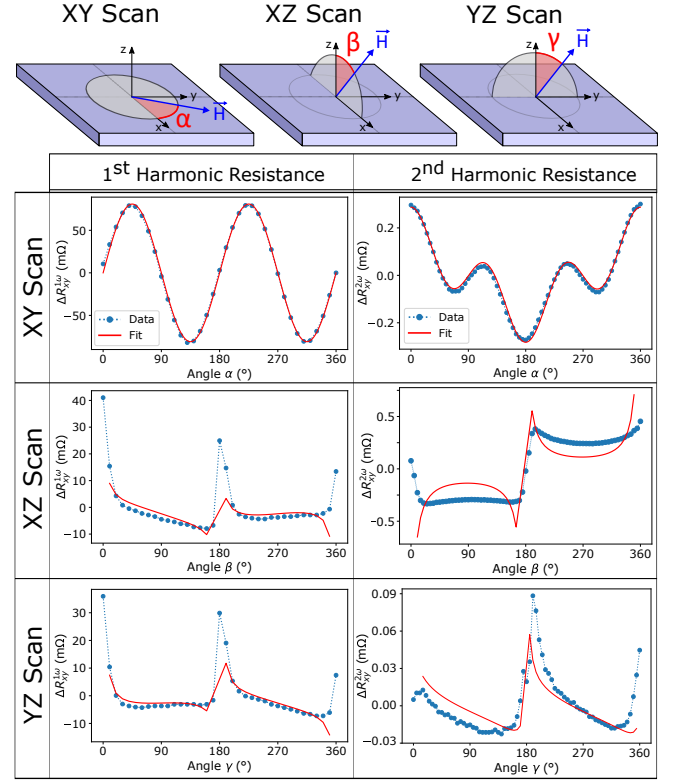


FIG. 2. Angular dependence of 1st and 2nd harmonic (columns) resistance signals in XY, XZ and YZ scans (rows) at $\mu_0 H = 3$ T. The current amplitudes are 100 μ A and 1.5 mA in the 1st and 2nd harmonic measurements, respectively. The blue dots are the data points whereas, the red line is the fit resulting from our model that is described in the main text. The geometry of magnetic field scans in the 3 principal planes (XY, XZ and YZ scans) and the definition of the angles α , β and γ are shown at the top. The magnitude of longitudinal SMR is approximately 0.02% and it is consistent with studies on similar AFM/HM systems [24, 28].

In the macrospin approximation, the free energy density (in field dimensions of Tesla) can be expressed as:

$$\frac{\epsilon}{\hbar \gamma} = H_{ex} \mathbf{m}_1 \cdot \mathbf{m}_2 + H_K [(e_h \cdot \mathbf{m}_1)^2 + (e_h \cdot \mathbf{m}_2)^2] - H_D \mathbf{e}_D \cdot (\mathbf{m}_1 \times \mathbf{m}_2) - \mathbf{H} \cdot (\mathbf{m}_1 + \mathbf{m}_2), \quad (2)$$

where γ is the gyromagnetic ratio. \mathbf{e}_h and \mathbf{e}_D are unit vectors in the directions of the hard axis anisotropy and DMI respectively. H_{ex} , H_K and H_D are the effective fields associated with the exchange interaction, the hard axis anisotropy and the DMI, respectively. Here we have ignored the in-plane easy axis anisotropy because it is much weaker than H_K and H_D [31]. This simplification, however, becomes invalid when the in-plane projection of \mathbf{H} is insufficient to maintain a single domain state [20] (e.g., when \mathbf{H} is nearly perpendicular to the easy plane). The dynamics of the sublattice magnetic moments are described by the coupled Landau-Lifshitz-Gilbert-Slonczewski equations:

$$\begin{aligned} \frac{d\mathbf{m}_{1,2}}{dt} = & \gamma \mathbf{H}_{1,2}^{\text{eff}} \times \mathbf{m}_{1,2} + \alpha_0 \mathbf{m}_{1,2} \times \frac{d\mathbf{m}_{1,2}}{dt} \\ & + \gamma [H_{\text{Oe}}(J_{\text{AC}}) + H_{\text{FL}}(J_{\text{AC}})] \boldsymbol{\sigma}_{\text{AC}} \times \mathbf{m}_{1,2} \\ & + \gamma H_{\text{DL}}(J_{\text{AC}}) \mathbf{m}_{1,2} \times [\mathbf{m}_{1,2} \times \boldsymbol{\sigma}_{\text{AC}}], \end{aligned} \quad (3)$$

where $\mathbf{H}_{1,2}^{\text{eff}} = -\delta\epsilon/(\hbar\gamma\delta\mathbf{m}_{1,2})$ is the effective field acting on $\mathbf{m}_{1,2}$, α_0 is the Gilbert damping constant, $H_{\text{Oe}}(J_{\text{AC}}) = \frac{1}{2}\mu_0 A_x J_{\text{AC}} t_{\text{Pt}}$ is the Oersted field and t_{Pt} the thickness of the Pt film. $\boldsymbol{\sigma}_{\text{AC}}$ is the direction of spin accumulation (here along \hat{y}), and $H_{\text{FL}}(J_{\text{AC}})$ and $H_{\text{DL}}(J_{\text{AC}})$ are the strengths of the field-like and damping-like torques, respectively.

All the three fields generated by the current are linearly proportional to J_{AC} . In particular, H_{Oe} and H_{FL} satisfy the same symmetry, but we show that Oersted field contribution is much smaller than field-like SOT, using finite-element simulations (see Supplementary Materials). Because the intrinsic frequency of the spin dynamics in α - Fe_2O_3 is many orders of magnitude larger than ω [33], we can treat $\mathbf{m}_{1,2}$ as quasi-static vectors that adiabatically adjust to the AC current, remaining in the instantaneous ground state in the presence of current-induced torques. Under the adiabatic approximation, Eq. (3) can be solved analytically [34], and, if $|\mathbf{m}| = |\mathbf{m}_1 + \mathbf{m}_2| \ll 1$, can be expressed by the Néel vector \mathbf{n} as function of J_{AC} and \mathbf{H} . Finally, by inserting $\mathbf{n}(J_{\text{AC}}, \mathbf{H})$ into Eq. (1), we obtain the general solution for the SMR and thus $V_{xy}^{1\omega}$ and $V_{xy}^{2\omega}$. This general solution, however, cannot be recast into a concise form unless we assume that $\mathbf{e}_h \parallel \hat{z}$ and $\mathbf{e}_D \parallel \hat{z}$ i.e. the easy plane coincides with the film plane without tilting. The special solution for vanishing tilt is:

$$R_{xy}^{1\omega} = -\frac{1}{2} R_0 \sin 2\phi_H, \quad (4)$$

$$R_{xy}^{2\omega} = R_0 \left[-\frac{\cos 2\phi_H \cos \phi_H}{H \sin \theta_H} (H_{\text{Oe}} + H_{\text{FL}}) + \right. \quad (5)$$

$$\left. \frac{2H_{\text{ex}} H \cos \theta_H \cos 2\phi_H \sin \phi_H H_{\text{DL}}}{2(H_D^2 + 2H_{\text{ex}} H_K) H \sin \theta_H + H_D(H^2 + 4H_{\text{ex}} H_K + H_D^2)} \right]$$

where $\theta_H \in [0, \pi]$ and $\phi_H \in [0, 2\pi]$ are the polar and azimuthal angles of \mathbf{H} , and R_0 is a current-independent constant. In Fig. 2, we identify these angles as $\theta_H = \pi/2$ and $\phi_H = \alpha$ for the XY scan, $\theta_H = \beta$ (or $2\pi - \beta$) and $\phi_H = 0$ (or $-\pi$) for the XZ scan, and $\theta_H = \gamma$ (or $2\pi - \gamma$) and $\phi_H = \pi/2$ (or $-\pi/2$) for the YZ scan, respectively. To better fit the data in Fig. 2, however, we further allow a small tilting of the hard axis but still assume that $\mathbf{e}_D \parallel \mathbf{e}_h$, which yields a complicated expression not shown here. We observe a good agreement with the experiment at a tilt angle of 3° with respect to \hat{z} , which is plotted by the red curves in Fig. 2. Since the model assumes $|\mathbf{m}| \ll 1$, our solution breaks down at extremely large fields, which is partially reflected in Fig. 3 and discussed later.

The field-like torque and the damping-like torque play very different roles in driving the dynamics of magnetic moments. As illustrated in Fig. 1(b), the damping-like torque cants both magnetic moments towards the same in-plane direction, which will subsequently leverage the exchange torque between \mathbf{m}_1 and \mathbf{m}_2 so that the Néel vector \mathbf{n} develops an out-of-plane component. By contrast, the field-like torque acts as an effective field that directly drives the net magnetic moment so that the AC current induces an in-plane rotation of \mathbf{m} . Since $\mathbf{m} \perp \mathbf{n}$ by definition, a direct consequence is that \mathbf{n} undergoes an in-plane oscillation. Correspondingly, in the absence of tilting, damping-like torques vanish in the XY scan ($\theta_H = 90^\circ$), and field-like torques vanish in YZ scan ($\phi_H = 90^\circ$). However, any amount of tilting of the easy plane will prevent this vanishing and both field-like and damping-like torques will have contributions in XY and YZ scans.

Because of the small magnetic moment present in α - Fe_2O_3 above its Morin transition, perpendicular coupling between the Néel vector and the external field is easily achievable at moderate field strengths. The easy plane and the external field direction together are adequate to uniquely set the equilibrium direction of the Néel vector and a $\gtrsim 1$ T in-plane component of the applied field can fully align the Néel vector to overcome any in-plane magnetic anisotropy.

We fit the experimental results with 3 free parameters: the direction of the hard axis (\mathbf{e}_h) and the amplitudes of the spin-orbit torques (H_{FL} and H_{DL}). For every scan, first we fit the 1st harmonic response, where we extract the current-independent constant R_0 (Eq. 4). Then together with the R_0 , we use material parameters from the literature $H_D = 2$ T, $H_K = 0.01$ T and $H_{\text{ex}} = 900$ T [35–37] to fit the responses with our model. These fits allow us to extract the amplitudes of effective fields associated with the spin-orbit torques per current density which are $H_{\text{FL}}/J_{\text{AC}} \approx 7.5 \times 10^{-2}$ T/(10^{12} A/m²) and $H_{\text{DL}}/J_{\text{AC}} \approx 4.2 \times 10^{-4}$ T/(10^{12} A/m²).

A slight tilting ($\sim 3^\circ$) of the hard-axis \mathbf{e}_h from the \hat{z} -direction is needed in order to simultaneously capture the form of each and every one of the field scans. This tilt is especially crucial in 1st harmonic out-of-plane scans (XZ and YZ), where in order to get any non-zero response from our model, we need some degree of canting of the easy plane. Moreover, to explain the shape of the response, an additional cosine term is needed, which we interpret as the ordinary Hall effect response of Pt.

There are also effects arising from the ordinary Hall effect induced by the perpendicular field component and from the spin Seebeck effect (SSE) due to a thermal gradient in the \hat{z} direction caused by Joule heating. Figure 3 summarizes how we extracted these contributions. On the left (Fig. 3(a) and (c)), we show the field dependence of 1st harmonic YZ and 2nd harmonic XY scans. And, on the right (Fig. 3(b) and (d)), we show the sep-

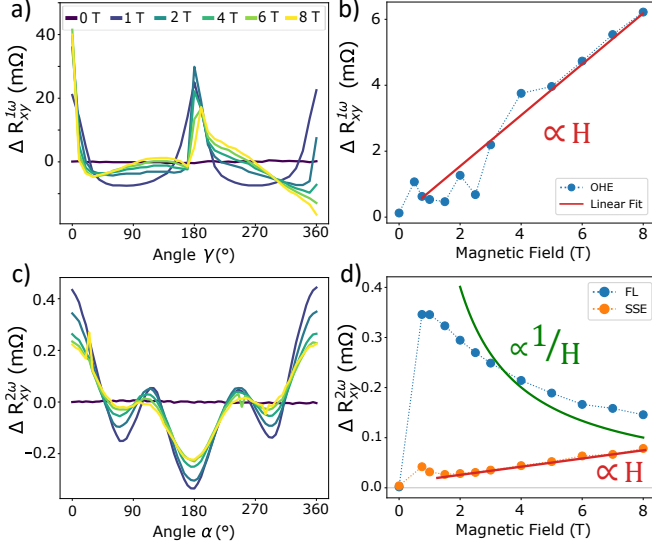


FIG. 3. Separating Hall effect and spin Seebeck effect contributions. a) Field dependence of 1st harmonic response in YZ scan, from 0 to 8 T as indicated by the legend. b) The Hall effect in 1st harmonic YZ scan (a), as a function of applied field. The linear trend line supports the claim that the origin of the signal is the ordinary Hall effect. c) Field dependence of 2nd harmonic response in XY scan, which shares the same legend as (a). d) Antiferromagnetic spin Seebeck effect (SSE) separated from field-like SOT in 2nd harmonic XY scan (c), as a function of applied field. The field-like component scales as $1/H$, whereas the SSE component scales linearly with H .

arated contributions of Hall effect and SSE from those scans, respectively. The field dependence of the signals can be used to isolate different contributions to the signal, as well as to show the model field dependence with the experimental results.

Figure 3(b) shows the Hall effect contribution in 1st harmonic and YZ scans. Since the expected Hall contribution is in the form $R_H^{1\omega} = H R_0^H \cos \theta$, the linear trend with applied field supports our claim. Similarly, Fig. 3(d) shows decomposition of $R_{xy}^{2\omega}$ into two components: Field-like SOT (blue) $R_{FL}^{2\omega}$ and spin Seebeck effect (orange) $R_{SSE}^{2\omega}$. In this case, the expected signals are of the form $R_{FL}^{2\omega} = H R_0^{FL} \cos 2\alpha \cos \alpha$ and $R_{SSE}^{2\omega} = H R_0^{SSE} \cos \alpha$ for field-like and SSE contributions, respectively. The form of the SSE contribution indicates that the effect is associated with the excess moment in the so called the transverse spin Seebeck geometry, in which the signal scales linearly with the applied field [38]. Furthermore, the remaining field-like component decreases with increasing applied magnetic field and follows a $1/H$ dependence, as in Eq. 5. We attribute the deviation from a $1/H$ dependence at low and high fields to the fact that our model assumptions are not valid in those limits.

Our experimental results show that the field-like torque is about two orders of magnitude larger than the damping-like torque, distinct from what is found in fer-

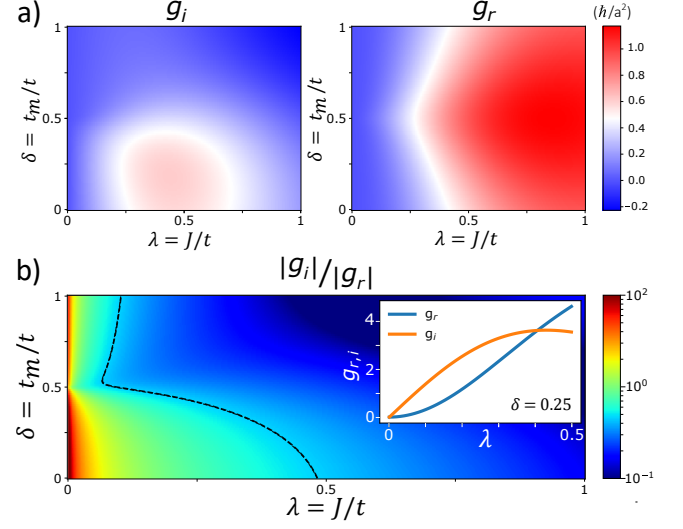


FIG. 4. a) Imaginary (left) and real (right) parts of the spin mixing conductance ($g = g_r + ig_i$) of an AFM/NM interface. The scale is indicated by the shared color bar on the right, with units of \hbar per unit area a^2 on the interface, where a is the lattice constant. b) Ratio of $|g_i|$ to $|g_r|$. As λ approaches zero $|g_i|$ dominates over $|g_r|$. The dashed line shows $|g_i| = |g_r|$, which separates the field-like torque dominating region ($g_i > g_r$) on the left from the damping-like torque dominating region ($g_r > g_i$) on the right. The color bar scale is logarithmic in this case. The inset shows a line cut of g_r and g_i vs. λ at $\delta=0.25$. Even though they both approach zero as λ goes to zero, g_r decreases faster than g_i and their ratio g_i/g_r diverges.

romagnets [39, 40]. This implies that in the spin mixing conductance $g = g_r + ig_i$ —which characterizes the spin transmission across the interface—the imaginary part g_i far exceeds the real part g_r , as $H_{DL} \sim g_r J_{AC}$ and $H_{FL} \sim g_i J_{AC}$ (see Supplementary Materials). To get at the origin of this unusual observation, we calculate g_i and g_r for a compensated interface by considering interfacial spin-dependent scattering processes, because electrons can deliver angular momenta to the magnetic moments near the interface through spin-flip scattering [11, 41], which manifests as spin torques exerting on the AFM. As detailed in Sec. 4 of the Supplementary Materials, the interfacial scattering here depends on three parameters: the electron hopping energy t in the NM (determined by the Fermi energy), the proximity-induced hopping t_m on the AFM side of the interface [42] and the interfacial exchange coupling J between conduction electrons in the NM and the magnetic moments in the AFM. In Fig. 4 we plot the dependence of g_r and g_i on two dimensionless parameters $\lambda = J/t$ and $\delta = t_m/t$.

We see from Fig. 4 that regions with small λ and δ have $g_i/g_r > 1$. This ratio can become extremely large when λ becomes even smaller, which, when comparing with our experiment, indicates that the Pt/ α -Fe₂O₃ interface just falls in the region of very small λ and δ . In

general, the ratio g_i/g_r can vary over a wide range of values depending on λ and δ , thus it is expected that the relative strength of the field-like and damping-like torques can vary significantly in different materials.

In conclusion, we determined the type and amplitude of SOTs in antiferromagnetic α -Fe₂O₃/Pt bilayers. An important finding is that the field-like torques are two orders of magnitude larger than damping-like torques, implying that the spin-mixing conductance of the α -Fe₂O₃/Pt interface has the unusual property of having a large imaginary component. It also points to magneto-elastic effects likely being the dominant mechanism of current-induced switching of the Néel vector of in α -Fe₂O₃ [8, 9, 28]. Our method can be extended to other AFM/HM systems by starting with the appropriate model and assumptions (e.g. magnetic anisotropies, DMI) to determine harmonic response [34]. Overall, our work demonstrates a way to quantify SOTs and opens up a promising path for future studies on similar AFM/HM heterostructures as well as a means that can be used in optimizing SOT on AFM for applications.

ACKNOWLEDGEMENT

This research was supported by the Air Force Office of Scientific Research under Grant FA9550-19-1-0307. The nanostructures were realized at the Advanced Science Research Center NanoFabrication Facility of the Graduate Center at the City University of New York.

-
- [1] E. V. Gomonay and V. M. Loktev, Spintronics of antiferromagnetic systems (Review Article), *Low Temperature Physics* **40**, 17 (2014).
- [2] T. Jungwirth, X. Marti, P. Wadley, and J. Wunderlich, Antiferromagnetic spintronics, *Nature Nanotechnology* **11**, 231 (2016).
- [3] V. Baltz, A. Manchon, M. Tsoi, T. Moriyama, T. Ono, and Y. Tserkovnyak, Antiferromagnetic spintronics, *Rev. Mod. Phys.* **90**, 015005 (2018).
- [4] S. Fukami, V. O. Lorenz, and O. Gomonay, Antiferromagnetic spintronics, *Journal of Applied Physics* **128**, 070401 (2020).
- [5] P. Wadley, B. Howells, J. Železny, C. Andrews, V. Hills, R. P. Campion, V. Novak, K. Olejnik, F. Maccherozzi, S. S. Dhesi, S. Y. Martin, T. Wagner, J. Wunderlich, F. Freimuth, Y. Mokrousov, J. Kune, J. S. Chauhan, M. J. Grzybowski, A. W. Rushforth, K. W. Edmonds, B. L. Gallagher, and T. Jungwirth, Electrical switching of an antiferromagnet, *Science* **351**, 587 (2016).
- [6] R. Cheng, D. Xiao, and A. Brataas, Terahertz Antiferromagnetic Spin Hall Nano-Oscillator, *Phys. Rev. Lett.* **116**, 207603 (2016).
- [7] I. Gray, T. Moriyama, N. Sivadas, G. M. Stiehl, J. T. Heron, R. Need, B. J. Kirby, D. H. Low, K. C. Nowack, D. G. Schlom, D. C. Ralph, T. Ono, and G. D. Fuchs, Spin Seebeck Imaging of Spin-Torque Switching in Antiferromagnetic Pt/NiO Heterostructures, *Physical Review X* **9**, 041016 (2019).
- [8] Y. Cheng, S. Yu, M. Zhu, J. Hwang, and F. Yang, Electrical Switching of Tristate Antiferromagnetic Néel Order in α -Fe₂O₃ Epitaxial Films, *Phys. Rev. Lett.* **124**, 027202 (2020).
- [9] E. Cogulu, N. N. Statuto, Y. Cheng, F. Yang, R. V. Chopdekar, H. Ohldag, and A. D. Kent, Direct imaging of electrical switching of antiferromagnetic Néel order in α -Fe₂O₃ epitaxial films, *Phys. Rev. B* **103**, L100405 (2021).
- [10] H. V. Gomonay and V. M. Loktev, Spin transfer and current-induced switching in antiferromagnets, *Phys. Rev. B* **81**, 144427 (2010).
- [11] R. Cheng, J. Xiao, Q. Niu, and A. Brataas, Spin pumping and spin-transfer torques in antiferromagnets, *Phys. Rev. Lett.* **113**, 057601 (2014).
- [12] C. O. Avci, K. Garello, M. Gabureac, A. Ghosh, A. Fuhrer, S. F. Alvarado, and P. Gambardella, Interplay of spin-orbit torque and thermoelectric effects in ferromagnet/normal-metal bilayers, *Phys. Rev. B* **90**, 224427 (2014).
- [13] S. Y. Bodnar, L. Šmejkal, I. Turek, T. Jungwirth, O. Gomonay, J. Sinova, A. A. Sapozhnik, H.-J. Elmers, M. Kläui, and M. Jourdan, Writing and reading antiferromagnetic Mn₂Au by Néel spin-orbit torques and large anisotropic magnetoresistance, *Nature Communications* **9** (2018).
- [14] X. Z. Chen, R. Zarzuela, J. Zhang, C. Song, X. F. Zhou, G. Y. Shi, F. Li, H. A. Zhou, W. J. Jiang, F. Pan, and Y. Tserkovnyak, Antidamping-torque-induced switching in biaxial antiferromagnetic insulators, *Phys. Rev. Lett.* **120**, 207204 (2018).
- [15] X. F. Zhou, J. Zhang, F. Li, X. Z. Chen, G. Y. Shi, Y. Z. Tan, Y. D. Gu, M. S. Saleem, H. Q. Wu, F. Pan, and C. Song, Strong Orientation-Dependent Spin-Orbit Torque in Thin Films of the Antiferromagnet Mn₂Au, *Phys. Rev. Applied* **9**, 054028 (2018).
- [16] A. Parthasarathy, E. Cogulu, A. D. Kent, and S. Rakheja, Precessional spin-torque dynamics in biaxial antiferromagnets, *Phys. Rev. B* **103**, 024450 (2021).
- [17] Q. Shao, P. Li, L. Liu, H. Yang, S. Fukami, A. Razavi, H. Wu, K. Wang, F. Freimuth, Y. Mokrousov, M. D. Stiles, S. Emori, A. Hoffmann, J. Akerman, K. Roy, J.-P. Wang, S.-H. Yang, K. Garello, and W. Zhang, Roadmap of spin-orbit torques, *IEEE Transactions on Magnetics* **57**, 1 (2021).
- [18] L. Zhu, D. C. Ralph, and R. A. Buhrman, Maximizing spin-orbit torque generated by the spin Hall effect of Pt, *Applied Physics Reviews* **8**, 031308 (2021).
- [19] L. Baldrati, A. Ross, T. Niizeki, C. Schneider, R. Ramos, J. Cramer, O. Gomonay, M. Filianina, T. Savchenko, D. Heinze, A. Kleibert, E. Saitoh, J. Sinova, and M. Kläui, Full angular dependence of the spin Hall and ordinary magnetoresistance in epitaxial antiferromagnetic NiO(001)/Pt thin films, *Phys. Rev. B* **98**, 024422 (2018).
- [20] Y. Cheng, S. Yu, A. S. Ahmed, M. Zhu, Y. Rao, M. Ghazisaeidi, J. Hwang, and F. Yang, Anisotropic magnetoresistance and nontrivial spin Hall magnetoresistance in Pt/ α -Fe₂O₃ bilayers, *Phys. Rev. B* **100**, 220408 (2019).
- [21] J. E. Hirsch, Spin hall effect, *Physical Review Letters* **83**, 1834 (1999).
- [22] G. Y. Guo, S. Murakami, T.-W. Chen, and N. Nagaosa, Intrinsic spin hall effect in platinum: First-principles calculations, *Physical Review Letters* **100**, 096401 (2008).
- [23] H. Nakayama, M. Althammer, Y.-T. Chen, K. Uchida, Y. Kajiwara, D. Kikuchi, T. Ohtani, S. Geprägs, M. Opel, S. Takahashi, R. Gross, G. E. W. Bauer, S. T. B. Goennenwein, and E. Saitoh, Spin hall magnetoresistance induced by a nonequilibrium proximity effect, *Physical Review Letters* **110**, 206601 (2013).
- [24] G. R. Hoogeboom, A. Aqeel, T. Kuschel, T. T. M. Palstra, and B. J. van Wees, Negative spin hall magnetoresistance of pt on the bulk easy-plane antiferromagnet NiO, *Applied Physics Letters* **111**, 052409 (2017).
- [25] Y.-T. Chen, S. Takahashi, H. Nakayama, M. Althammer, S. T. B. Goennenwein, E. Saitoh, and G. E. W. Bauer, Theory of spin Hall magnetoresistance, *Phys. Rev. B* **87**, 144411 (2013).
- [26] T. Taniguchi, J. Grollier, and M. Stiles, Spin-transfer torques generated by the anomalous hall effect and anisotropic magnetoresistance, *Physical Review Applied* **3**, 044001 (2015).
- [27] C. Schmitt, L. Baldrati, L. Sanchez-Tejerina, F. Schreiber, A. Ross, M. Filianina, S. Ding, F. Fuhrmann, R. Ramos, F. Maccherozzi, D. Backes, M.-A. Mawass, F. Kronast, S. Valencia, E. Saitoh, G. Finocchio, and M. Kläui, Identification of Néel Vector Orientation in Antiferromagnetic Domains Switched by Currents in NiO/Pt Thin Films, *Phys. Rev. Applied* **15**, 034047 (2021).
- [28] P. Zhang, J. Finley, T. Safi, and L. Liu, Quantitative study on current-induced effect in an antiferromagnet insulator/pt bilayer film, *Phys. Rev. Lett.* **123**, 247206 (2019).
- [29] M. Hayashi, J. Kim, M. Yamanouchi, and H. Ohno, Quantitative characterization of the spin-orbit torque us-

- ing harmonic Hall voltage measurements, Phys. Rev. B **89**, 144425 (2014).
- [30] J. Fischer, O. Gomonay, R. Schlitz, K. Ganzhorn, N. Vlietstra, M. Althammer, H. Huebl, M. Opel, R. Gross, S. T. B. Goennenwein, and S. Geprägs, Spin Hall magnetoresistance in antiferromagnet/heavy-metal heterostructures, Phys. Rev. B **97**, 014417 (2018).
- [31] R. Lebrun, A. Ross, O. Gomonay, S. A. Bender, L. Baldtrati, F. Kronast, A. Qaiumzadeh, J. Sinova, A. Brataas, R. A. Duine, and M. Kläui, Anisotropies and magnetic phase transitions in insulating antiferromagnets determined by a Spin-Hall magnetoresistance probe, Communications Physics **2**, 50 (2019).
- [32] We note that contribution to R_{xy} of the form $m_x m_y$ is negligible.
- [33] M. Seavey, Acoustic resonance in the easy-plane weak ferromagnets α -Fe₂O₃ and FeBO₃, Solid State Communications **10**, 219 (1972).
- [34] H. Zhang and R. Cheng, Theory of the harmonic hall responses of spin-torque driven antiferromagnets, arXiv.org 10.48550/ARXIV.2112.12772 (2021).
- [35] S. J. Williamson and S. Foner, Antiferromagnetic Resonance in Systems with Dzyaloshinsky-Moriya Coupling; Orientation Dependence in α -Fe₂O₃, Phys. Rev. **136**, A1102 (1964).
- [36] K. Mizushima and S. Iida, Effective in-plane anisotropy field in α -Fe₂O₃, Journal of the Physical Society of Japan **21**, 1521 (1966).
- [37] P. R. Elliston and G. J. Troup, Some antiferromagnetic resonance measurements in α -Fe₂O₃, Journal of Physics C Solid State Physics **1**, 169 (1968).
- [38] G. E. W. Bauer, E. Saitoh, and B. J. van Wees, Spin caloritronics, Nature Materials **11**, 391 (2012).
- [39] Y. Tserkovnyak, A. Brataas, and G. E. Bauer, Spin pumping and magnetization dynamics in metallic multilayers, Physical Review B **66**, 224403 (2002).
- [40] K. Xia, P. J. Kelly, G. Bauer, A. Brataas, and I. Turek, Spin torques in ferromagnetic/normal-metal structures, Physical Review B **65**, 220401 (2002).
- [41] R. Cheng, *Aspects of antiferromagnetic spintronics*, Ph.D. thesis, The University of Texas at Austin (2014).
- [42] In AFM, the spin and sublattice degrees of freedom are locked together. Therefore, a spin-flip scattering must involve electron hopping between the two sublattices on the AFM side of the interface. Since the AFM is insulating by itself, such a process must rely on the proximity-induced t_m .